IEEE Access
Multidisciplinary | Rapid Review | Open Access Journal

Received 27 February 2024, accepted 6 March 2024, date of publication 16 April 2024, date of current version 2 May 2024.

Digital Object Identifier 10.1109/ACCESS.2024.3385864

RESEARCH ARTICLE

An Optimized Data and Model Centric Approach for Multi-Class Automated Urine Sediment Classification

SANIA AKHTAR[1], MUHAMMAD HANIF[2], AHMAR RASHID[1], KHURSHEED AURANGZEB[3], (Senior Member, IEEE), EJAZ AHMAD KHAN[4], HAMDI MELIH SARAOGLU[5], AND KAMRAN JAVED[6]

[1]Faculty of Computer Science and Engineering, Ghulam Ishaq Khan Institute of Engineering Sciences and Technology, Topi 23460, Pakistan
[2]Kobayashi Research Laboratory, Information Technology Center, The University of Tokyo, Tokyo 113-0032, Japan
[3]Department of Computer Engineering, College of Computer and Information Sciences, King Saud University, Riyadh 11543, Saudi Arabia
[4]Department of Public Health, Health Services Academy, Islamabad 23000, Pakistan
[5]Department of Electrical and Electronics, Kütahya Dumlupınar University, 43100 Kutahya, Turkey
[6]National Centre of Artificial Intelligence (NCAI), Saudi Data and Artificial Intelligence Authority (SDAIA), Riyadh 11543, Saudi Arabia

Corresponding author: Muhammad Hanif (muhammad.hanif@giki.edu.pk)

This Research is funded by Researchers Supporting Project Number (RSPD2024R947), King Saud University, Riyadh, Saudi Arabia.

ABSTRACT Automated urine sediment analyzers play a crucial role in diagnosing urinary tract infections, offering real-time data analysis and expediting patient diagnosis. This paper introduces a novel hybrid approach combining data-centric and model-centric techniques for automated urine sediment analysis. The proposed methodology addresses challenges such as morphological similarities among particle classes, uneven particle distribution, and intra/inter-class variations. A modified version of convolutional neural network (CNN), specifically the Visual Geometry Group (VGG-19) model, incorporating transfer learning, along with data augmentation is proposed for automated urine sediment classification with 98% accuracy and impressive inference time of 61ms per image. The proposed approach outperforms existing methods, especially in handling diverse sediment categories, demonstrating its potential for practical applications in medical diagnostics. We proposed the integration of a data-centric approach for improved labeling reliability and a model-centric approach for fine-tuning of the deep learning model, showcasing promising results in recognizing 12 distinct urine sediment classes. This study also emphasizes the importance of collaboration with medical professionals in refining the model's performance and handling challenges related to data acquisition and class imbalance. The proposed approach provides a significant advancement in automating and enhancing urine sediment analysis processes.

INDEX TERMS Data-centric, microscopic images, urine sediment, model-centric, vitro examination, automated urine sediment analyzer.

I. INTRODUCTION

The microscopic scrutiny of urinary sediments stands as a widely employed and indispensable diagnostic laboratory screening test, providing valuable insights into a myriad of metabolic, nephrogenic, and urological conditions. This examination entails the analysis of urinary cell morphology, both cellular and noncellular casts, the enumeration of white blood cells (WBCs) and red blood cells (RBCs), and the identification of endogenous crystals. These parameters hold paramount importance in the assessment of various acute or chronic medical conditions [1], [2], [3], [4]. Moreover,

The associate editor coordinating the review of this manuscript and approving it for publication was Chao Zuo.

© 2024 The Authors. This work is licensed under a Creative Commons Attribution-NonCommercial-NoDerivatives 4.0 License.
For more information, see https://creativecommons.org/licenses/by-nc-nd/4.0/

the identification and measurement of protein or sugar in urine serve as crucial indicators in diagnosing several kidney-related ailments, particularly kidney failure [5]. Regrettably, conventional microscopic examination-based methods for urine sediment analysis suffer from inefficiency and subjectivity, rendering them error-prone and time-consuming [6], [7]. The main urine sediments and their subclasses are shown in Figure 1. The introduction of automatic urine analyzers in certain hospitals has significantly improved clinical practices by reducing analysis time and enhancing the efficiency of medical professionals. These analyzers contribute to smart healthcare systems by enabling real-time data transmission and analysis, thereby minimizing the risk of human error and ensuring more reliable diagnoses. As a result, these machines have become an integral component of modern healthcare, streamlining urine analysis processes. In contrast to general object recognition, urine sediments pose a challenge due to their relatively fewer distinctive features that are not easily discernible by humans. Additionally, specific categories of urine sediments exhibit noticeable similarities. Consequently, research efforts have been directed towards automating urine sediment analysis to enhance diagnostic capabilities and overcome the limitations associated with manual examination [8], [9]. Automated urine analysis relies on digital images of urinary sediments captured through a microscopic lens. The process involves three main steps: segmentation, feature extraction, and classification [10], [11]. Object segmentation is crucial for identifying and distinguishing individual cell types and sediments [12], [13]. The effectiveness of these methods depends on precise target segmentation and the efficient selection and combination of relevant features, as emphasized in previous studies [3], [5]. Deep learning models, particularly convolutional neural networks (CNNs) [14], [15], [16], [17], have emerged as pivotal tools in image recognition. Unlike conventional feature extraction methods, CNNs offer the advantage of automatically extracting a comprehensive set of features and optimizing their combination [18], [19]. To explore the unique characteristics of urine sediment images, this study proposes an innovative approach that harnesses the power of four distinct CNN models, enabling rapid and precise recognition of urine sediments [20], [21]. This method effectively addresses the challenge of distinguishing particles with similar morphological structures that had previously caused confusion.

A. MOTIVATION

Table. 1 details the summary of the recent models of automated urine sediment analysis. Our motivation to novel hybrid approach that combines data-centric and model-centric techniques to optimally tune the deep learning model parameters and apply error analysis-driven iterations to address class imbalance issues in urine sediment data, is based on these models. Each model, individually, motivated our novel model:

1) DATA-CENTRIC APPROACH

Motivation: Leveraging the success of recent models like [3] and [4] through data augmentation, our hybrid approach prioritizes a data-centric strategy to improve the data. By carefully curating a comprehensive dataset and applying advanced augmentation techniques, we aim to enhance the model's ability to generalize and accurately classify diverse urine sediment components.

2) MODEL-CENTRIC TECHNIQUES

Motivation: Inspired by the diverse model architectures used by [5], [18], and [22], our hybrid approach integrates model-centric techniques to refine the architecture and parameters. This ensures that the deep learning model is well-suited to capture intricate patterns in urine sediment images, fostering improved recognition of classes and overall model performance.

3) ERROR ANALYSIS-DRIVEN ITERATIONS

Motivation: Building on the experiences of recent models such as [19] and [23], our approach incorporates an error analysis-driven iteration process. By systematically analyzing model errors, we aim to identify and address class imbalance issues within urine sediment data. This iterative refinement process is designed to specifically target areas where the model may struggle, leading to enhanced accuracy and reliability in automated urine sediment analysis.

4) HYBRID OPTIMIZATION FOR CLASS IMBALANCE

Motivation: Recognizing the challenges posed by class imbalance, evident in models like [5] our hybrid approach is strategically designed to tackle these issues head-on. Through a combination of data-centric technique and model-centric adjustments, we strive to balance class representation, ensuring that the model is equally proficient in distinguishing both prevalent and less frequent components in urine sediment samples.

5) PERFORMANCE IMPROVEMENT FOCUS

Motivation: In light of the success achieved by recent models in various aspects, our hybrid approach is motivated by a strong focus on performance improvement. By synergizing data-centric and model-centric strategies and addressing class imbalance through error analysis-driven iterations, we anticipate a substantial enhancement in the overall efficiency and accuracy of automated urine sediment analysis, contributing to advancements in diagnostic capabilities. The key contributions of this study can be succinctly summarized as follows:

B. CONTRIBUTIONS/NOVELTIES

- **Optimal Approach to Urine Sediment Classification:** This work addresses urine sediment classification through a combination of data-centric and model-centric approaches. The data-centric approach involves

TABLE 1. Summary of the recent models of automated urine sediment analysis.

Authors	Number of Images	Number of Classes	Method
Erten [3]	5376	7 : Cast, Crystal, Ep, Ep nuclei, WBC, RBC, and Mycete	ACM mixer and DenseNet201
Li [4]	300,000	10 : RBC, WBC, WBC cluster, squamous EP, sperm, CAOX, hyaline cast, mucous, BACT, yeast	Data augmentation, area feature algorithm, AlexNetbased end-to-training CNN
Yildirim [5]	8509	8 : BACT, cluster, cylinder, Ep, WBC, RBC, Yeast, Others	Resnet50 + LBP + mRMR + SVM
Q.ji [18]	453,283	16	US-RepNet
Hilal [19]	9,004	7 : WBC, RBC, WBCC, Ep, Flat Ep, Mucs, Bubbles	Yolov7
Liang [22]	5377	7 : RBC, WBC, EP, EP nuclei, cast, crystals, mycete	DenseNet features a pyramid network
Akhtar [23]	5632	10 : RBC, WBC, casts, crystals, epithelial cells (epith), transitional epithelial cells (epithn), erythrocytes (eryth), leukocytes (leuko), and mycete & platelets.	Yolov8

sanity checks on data without altering the model, while the model-centric approach enhances the model's architecture while preserving its foundational blueprint.

- **Modification of VGG19 Architecture:** The VGG19 vanilla architecture was tailored to the specific problem at hand, leading to a significant reduction in model complexity. To combat overfitting and enhance generalization capability, a Euclidean norm was incorporated as a regularizer.
- **Creation of a Comprehensive Training Dataset:** A large collection of microscopic urine sediment images was meticulously labeled with professional assistance, forming a valuable training dataset. To address class imbalances in certain categories, transfer learning and data augmentation techniques were employed.
- **Two-Stage Cascaded Classification Model:** To address confusion among morphologically similar particles, a two-stage cascaded classification model was proposed. This cascaded model contributes to improving the discriminating accuracy of challenging sediment categories.
- **Impressive Performance:** The proposed network achieves an impressive 98% accuracy and operates with remarkable efficiency, taking only 61 ms to recognize each segmented image.

The subsequent sections of the paper are organized as follows: Section II provides a review of related literature, and Section III outlines the proposed methodology, elucidating the cascaded CNN models. In Section IV, we detail the experimental setup, and evaluate the performance of the proposed method, and Section V offers an in-depth discussion of the results and their implications. Finally, Section VI concludes the paper by summarizing the key findings and contributions to the field.

II. RELATED WORK

Deep learning, particularly Convolutional Neural Networks (CNNs), has made significant strides in various domains, primarily focusing on image recognition inspired by natural vision mechanisms. These techniques are broadly categorized into classifications and detection methods [23]. Formal methods classify the content of an image into predefined object classes, while the latter methods combine classification with object localization. In 2023, Erten et al. [3] integrated an Arnold Cat Map (ACM)-based mixer algorithm with transfer learning using DenseNet201 [24], [25]. Their model comprises four layers: (1) ACM-based mixer for generating mixed images, (2) DenseNet201 for feature extraction, (3) iterative neighborhood component analysis for feature selection, and (4) shallow kNN-based classification with ten-fold cross-validation. They achieved an impressive 98.52% accuracy for a seven-class problem. Ji et al. [4] proposed an integrated deep learning model, combining AlexNet and an Area Feature algorithm (AFA) module, significantly enhancing discrimination accuracy between challenging sediment categories. The combined network achieved an impressive 96.75% accuracy and required only 6.8 milliseconds to recognize a segmented image. In 2023, Yildirim et al. [5] proposed a hybrid image classification model that integrated textural analysis with CNN techniques. Combining features from textural analysis-based methods and CNN-based architectures using mRMR [26], [27], they achieved 96% accuracy for an eight-class problem. Research works [28], [29], and [30] employed feature extraction involving ResNet50, local binary pattern, and machine learning classifiers for classification. In 2022, Ji et al. [18] presented a semi-supervised learning method using US-RepNet for complex feature extraction from low-resolution urine sediment images. They integrated

a dual attention module to enhance fine-grained feature extraction and optimized the cross-entropy loss function for training an unbiased classifier, achieving a 94% accuracy for 16 classes. Nagai et al. [31] conducted a study focusing on the examination of urinary sediment crystals in medical screenings, improving efficiency by enhancing the image dataset and utilizing CNN for analysis. Their best model achieved 91.8% accuracy through diverse training techniques, showcasing the potential of deep learning-based crystal image classification in clinical applications, even with limited imaging data. Atıcı et al. [19] employed the Yolov7 deep learning algorithm to process microscopic images of urine sediments. They conducted seven clinically relevant cell segmentation and classification studies. The Yolov7 algorithm successfully segmented urine cell images, achieving a mean classification accuracy of 0.822 for all classes Akhtar et al. [23] recently utilized YoloV8 [32] to accurately detect and categorize urine particles, introducing a data-centric strategy to enhance dataset quality by addressing issues such as missing data, incorrect labeling, and class imbalance. Experimental results demonstrated that YOLOv8 outperforms existing techniques, achieving a mean average precision of 91% for eleven categories of urine sediments, with an average detection time of 0.6 ms. Li et al. [33] employed a combination of Faster RCNN [34] to detect urine erythrocytes were the focus of Li et al.'s study, where their model, trained on a dataset comprising 3969 images, achieved an impressive recall rate of up to 99.8% for five types of urine erythrocytes. Despite these promising outcomes, many models proposed in the literature encounter difficulties in distinguishing between structurally similar urine cell classes, such as squamous and non-squamous epithelial cells. Additionally, these models face challenges arising from inherent attributes of microscopic urine images, including reduced contrast, plain backgrounds, and densely packed particles. Consequently, accurately distinguishing diverse particle types proves highly challenging, especially in the context of various patient samples and intricate particle categories.

III. PROPOSED METHODOLOGY

The microscopic images of urine sediments are influenced by both physiological features of the urinary system and the physical properties of microscopic equipment. This gives rise to several research challenges:

- **Morphological Similarities:** Certain particle classes exhibit morphological similarities, such as the resemblance between RBCs and WBCs, making accurate identification challenging due to their small size and low image quality.
- **Uneven Distribution:** The uneven distribution of urine sediment particles in microscopic images across different urine samples introduces variability.
- **Intra and Inter-Class Variations:** Morphological variations within and between particle classes (e.g., squamous and non-squamous epithelial cells, subcategories of yeast, casts, crystals, epithelial cells, and bacteria) pose challenges for network generalization capabilities.

To address these challenges, this research employs the following strategies:

1. Data-Centric Approach: To address morphological similarities, a data-centric approach is adopted. Professional verification is utilized to resolve labeling errors within classes, enhancing the accuracy of identification.

2. Pre-processing Step: A pre-processing step is employed to segment micro-images of urine sediment particles into smaller, uniquely labeled images. This segmentation significantly reduces the time required for particle traversal, convolution, and classification [35].

3. Feature Extraction using VGG19: To handle intra and inter-class variations, the VGG19 architecture, known for its depth, is employed for feature extraction. Regularization techniques and dropout are incorporated to improve generalization by reducing model complexity.

4. Comprehensive Classification Method: A urine sediment image recognition method is developed with four components:

- Primary Network Module: A modified VGG19 identifies images across nine categories.
- RBC-WBC Classifier: A specialized classifier for distinguishing between red and white blood cells.
- Squa-Non Squa Classifier: A classifier for discriminating between squamous and non-squamous epithelial cells.
- HC-UC Binary Recognition Module: A module for binary recognition of high-contrast and low-contrast images.

Results from these modules are combined to provide a comprehensive classification outcome. The proposed methodology effectively addresses morphological similarities, uneven distribution, and intra/inter-class variations, contributing to improved urine sediment analysis and solve the problem of miss-classification. The proposed approach involves two important steps: the Data-Centric approach and the Model-Centric approach, represented in Figure. 2 and described in subsections B & C. The comprehensive workflow of the proposed model is delineated in subsection A.

A. SYSTEM MODEL

The entire work of the proposed methodology is comprised of the following five major steps. The flowchart of the workflow and pseudocode for the proposed methodology are provided by Figure. 3 and Tabel 2.

1) WORKFLOW STAGES

Step1:Input images

Step 2:Data labeling & data augmentation for 12 classes

Step 3: Data-Centric Approach

- Error Analysis

1) Identify incorrect labels
2) Identify the missing data points

- Improved the data
  1) If errors are found in the previous step, then proceed to the following steps:
     a) Correct labels with the assistance of medical professionals
     b) Label the missing data points
     c) Some classes exhibit a lower count in comparison to others; for instance, RBC and WBC are more abundant, whereas sperm and unknown casts are infrequent. In this case, acquire more data to increase the number of infrequent classes
- Validate data
  1) Verify the data for errors to ensure its accuracy and correctness.
- Repeat step 2 until urine sediment data is cleaned and verified

Step 4: Model Centric Approach

- Input: Cleaned & Verified urine data
- Training with initial parameters
- Evaluation
  1) During the testing phase, if the particles are correctly classified, stop the processes; otherwise, engage in different hyperparameter tuning to achieve the desired results.

Step 5:Cascaded Model

- In the first phase cleaned and verified dataset is given to the modified VGG19(main module) for the classification of nine categories
- In the second phase the RBC & WBC, squmouse & non sequamous epithelial cells, and hyaline cast & unknow cast are further classified by the submodules to solve the confusion between the particles.

B. DATA-CENTRIC APPROACH

Key Objectives of the Data-Centric Approach:

1. Improve Labeling Reliability: The approach aims to enhance the accuracy and reliability of labeling by addressing issues related to mislabeling or errors in the training dataset.

2. Eliminate Noise: By actively identifying and rectifying missing data and inaccuracies, the approach ensures the removal of noise from the dataset, resulting in a cleaner and more reliable training set.

3. Utilize High-Quality Data: The focus is on utilizing high-quality, accurate data for training, which is pivotal for the development of effective deep learning models. [23].

1) PROCESS OVERVIEW

1. Comprehensive Data Examination: The approach involves a meticulous examination of the training data, facilitated by the active participation of a team of medical professionals. This collaborative effort ensures a detailed understanding of the dataset.

2. Collaboration with Medical Professionals: Building upon existing research, collaboration with medical professionals is emphasized. This collaborative effort, as exemplified by Goswami et al.'s work in 2021 on urine analysis [36], [37] everages domain expertise to refine the dataset. Outcome: The collaborative and comprehensive Data-Centric approach enables the successful differentiation among twelve distinct categories of urine sediments. Figure. 4. summarizes the distinguishing features that result from this approach. The enriched dataset, verified and refined through collaboration,

TABLE 2. Pseudocode for the proposed method.

Algorithm: Urine Sediment Classification

Input:
Urine sediment dataset USD
Output:
Classified particles P, Classifier weights W
Data_lab & Data_Aug
Data Centric Approach
  for iteration = 1 to max-iteration **do**
    Error = $\text{Error}_A + \text{Error}_B$
    If Error > 0: **do**
      C_labels = rectified labels
      F_data_Points = Labeled missing data-pints
      Acquire_ additional data = labeled more data
      $\text{Validated\_Data} = \begin{cases} \text{Data} & \text{if Confirmed\_Error\_Free} = 1 \\ \text{Null} & \text{if Confirmed\_Error\_Free} = 0 \end{cases}$
    else:
      Exit_Loop $= 1$
  end for
Model Centric Approach:
  Parameter Initialization
    batch_size $= 256$
    num_classes $= 12$
    optimizer = RMSprop
    activation_function $= ReLU$
    momentum = 0.9
    epochs = 100
    pateince = 30
    lr_scheduler = 1e-5 $\times (0.5 \times \left\lfloor \frac{\text{epoch}}{5} \right\rfloor)$
  Testing Phase
    Input Image: For $i = 1, 2, 3, \ldots, n$ **do**
    Stage 1 (Main Module):
      Nine_Particle_classification
    Stage 2 (Submodule):
      Six_Particle_classification (to resolve the confusion)
Evaluation
  for iteration = 1 to max-iteration **do**
    if Particles_Correctly_Classified = 1
      then stop = 1
      else
        Perfrom Parameter Optimization
          Exit_Loop $= 0$ (until desired_results achieved)
          else
            Exit_Loop $= 1$
    end for
Returned the classified particles P, classifier weights W

Error_A = Identify incorrect labels, Error_B = Identify missing data points, C_labels = corrected labels, F_data_Points = Fix data points
Error = $\text{Error}_A + \text{Error}_B$

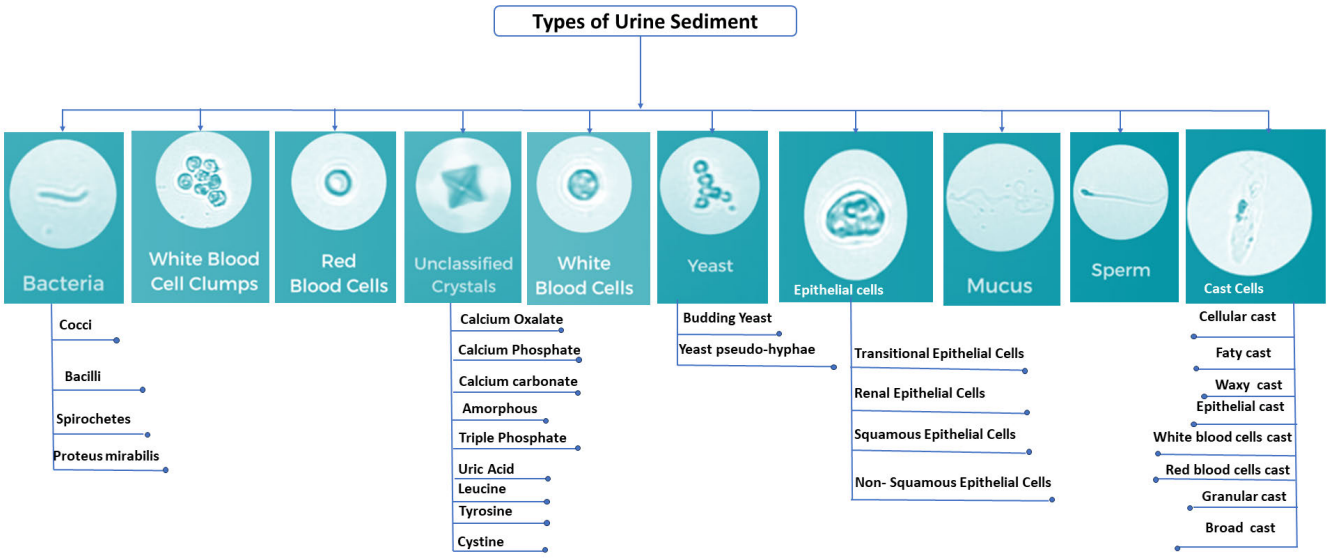

FIGURE 1. Illustration of urine types and their subtypes.

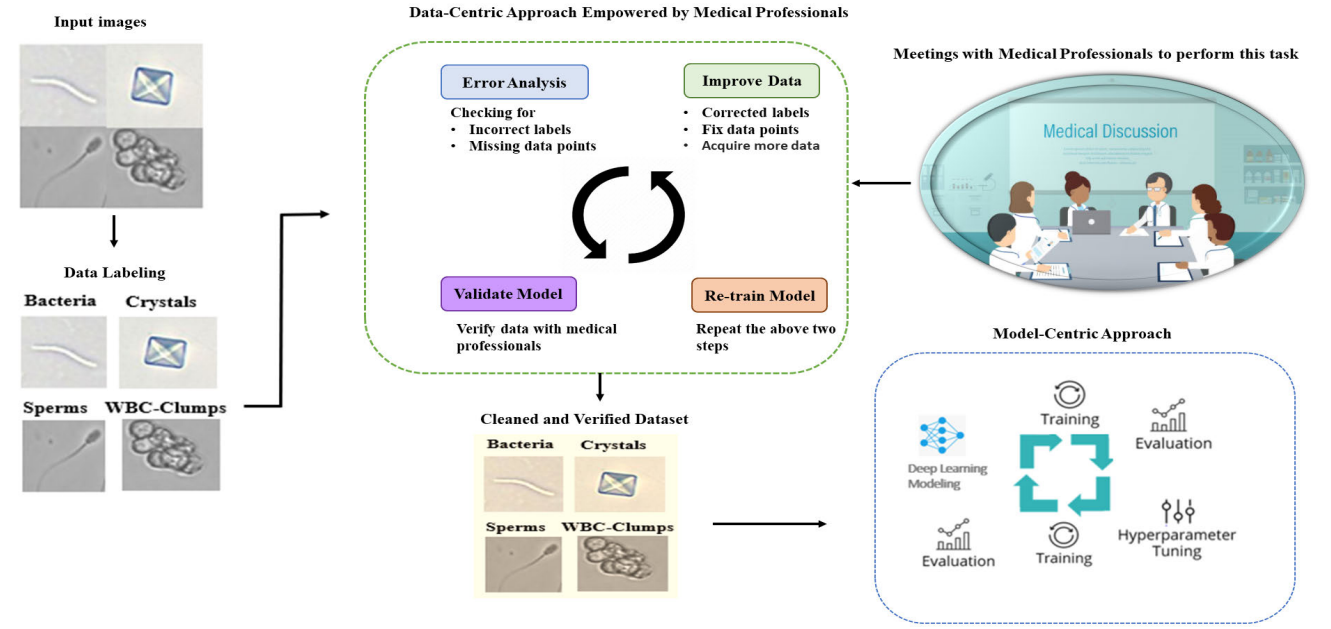

FIGURE 2. Representation of the combined Data-Centric & Model-Centric Approach.

forms the foundation for robust model training and improved outcomes in urine sediment analysis.

C. MODEL-CENTRIC APPROACH

The model-centric method is integral to the fine-tuning of deep learning models. This approach focuses on iteratively improving the model while maintaining a static dataset. Through architectural improvements and hyperparameter adjustments, the training workflow of the model is enhanced to achieve better performance and accuracy. Components of the Deep Learning Model Architecture are given below:

1. Core Network-Modified VGG19: Responsible for classifying nine categories, including bacteria, RBC-WBC, yeast, sperm, epithelial cells, cast cells, WBC-clumps, crystals, and mucus.

2. Sub-Modules:

- **RBC-WBC Classifier:** Specializes in distinguishing between Red Blood Cell (RBC) and White Blood Cell (WBC) particles.

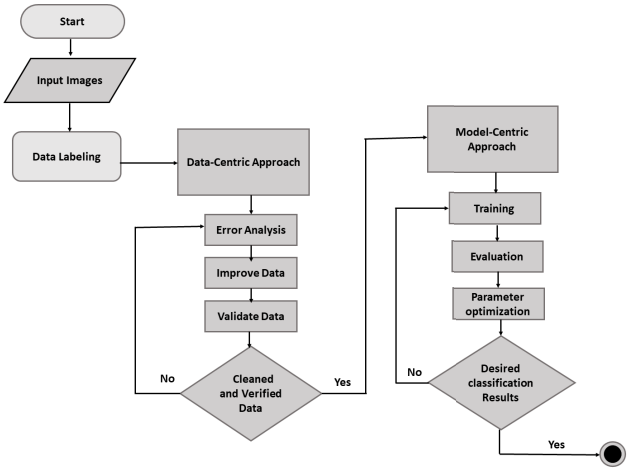

FIGURE 3. Workflow of the proposed methodology.

- **Squa-Non Squa Classifier:** Focuses on distinguishing between Squamous and Non-Squamous cells.
- **HC-UC Classifier:** Deals with the classification of Hyaline and Unknown casts.

1) WORKFLOW OVERVIEW

- **Modified VGG19 Core Network:** Classifies particles into nine categories.
- **Sub-Modules:** Specialized modules handle specific classifications based on particle types.
- **Collaborative Classification:** Outputs from sub-modules are combined to provide a comprehensive classification result.
- **Graphical Representation:** Figure. 5 illustrates a graphical representation of the model-centric classification architecture, showcasing the interplay between the core network and specialized sub-modules. The Model-Centric method, through its iterative improvements, contributes to the overall accuracy and performance of the deep learning model, making it well-suited for the nuanced challenges in urine sediment analysis.

2) MODEL IMPLEMENTATION AND OPTIMIZATION STRATEGIES

Modified VGG19 Architecture: This study adopts the modified VGG19 architecture for its classification tasks, leveraging its simplicity, ease of implementation, and robust feature learning capabilities. The modified VGG19 is chosen for its ability to capture both low-level details (e.g., edges and textures) and high-level features (e.g., object shapes and patterns), contributing significantly to overall performance. Key advantages of the modified VGG19 include impressive generalization capabilities, making it suitable for real-world applications. Figure. 6 demonstrates the architecture of modified VGG19 for main-network and also for sub-network.

TABLE 3. Main model configuration parameters.

Parameter	Value
Input Size	224x224
Model Parameters	33,220,041
Epochs	100
Batch Size	256
Optimizer	RMSprop
Activation Function	ReLU
Momentum	0.9
Learning rate scheduler	$1e-5 \times (0.5 * (\text{epoch}//5))$
Patience	30

a: TRANSFER LEARNING

Urine sediment recognition faces challenges due to imbalanced datasets and limited diversity. To overcome this, the study employs transfer learning [22], [38], initializing the model with VGG19 weights pre-trained on ImageNet [39], [40]. This strategy leverages learned features, optimizes computation, and enhances performance, especially in scenarios with limited data. Transfer learning involves freezing most layers, leaving only the last three convolutional blocks trainable, ensuring the model adapts to specific tasks.

b: DATA AUGMENTATION

Given the diverse distribution of sediment particles, data augmentation is employed to balance the dataset. Six augmentation techniques, including flipping, rotation, blurring, cropping, zooming, and noise creation, are utilized to enhance the representativeness of the dataset [41], as illustrated in Figure 7. Augmentation aims to enhance recognition metrics, particularly for rare occurrences like sperm and unknown casts [42], [43], contributing to better model generalization.

c: HYPER PARAMETERS FINE-TUNING

The modified VGG19 architecture undergoes meticulous fine-tuning to address potential overfitting and enhance generalization. Regularization techniques, including L2 regularization, are incorporated. Complexity reduction involves adjusting the number of neurons in the last two dense layers from 512 to 128. Batch normalization layers ensure stability, and a learning rate scheduler optimizes the training process. Table. 3 provides additional insights into the architecture.

3) SUB-MODULES (RBC-WBC, SQUA-NON SQUA, HC-UC CLASSIFIER

These specialized classifiers, integrated into the overall architecture, address confusion within specific particle classes. Adjustments in neurons, dropout rates, regularization techniques, and learning rate schedules enhance their effectiveness in resolving classification challenges. The Sub-Modules contribute to the collaborative classification results.

Conclusion: The model-centric approach, involving both the core network and specialized sub-modules, reflects a comprehensive strategy for refining and optimizing deep learning models in the context of urine sediment analysis. The

Sr#	Urine Sediments	Description	Distinguishing features	Sr#	Urine Sediments	Description	Distinguishing features
1	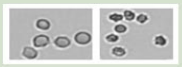	RBC	• Smooth outer surface/regular shape • Size varies from 6 – 8 µm in diameter. • Darker in color	7		WBC Clumps	• Bunch of WBC
2		WBC	• Irregular shape • Size varies from 12 – 17 µm in diameter. • Lighter in color	8		Sperms	• Thread like structure with black head
3	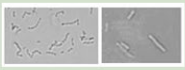	Bacteria	• Thread like structure • Black/white color	9	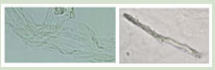	Mucus	• Thick , slippery fluid
4	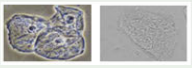	Squamous Epithelial Cells	• Smaller nuclei • Flat and sheet-like in appearance. • Larger size • Irregular cell borders	10	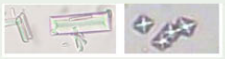	Crystals	• Chemical solidify into salt crystals • Dimond/prism/hexagon shape/round discs
5	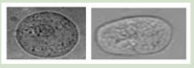	Non-Squamous Epithelial cells	• Larger nuclei • Round appearance • Smaller as compared to SEC • Regular Cells borders	11		Unknown Casts	• Tube/cylindrical shaped • Darker in color • Made of WBC
6	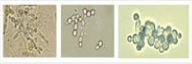	Yeasts	• Pale-green in colors • Well-defined walls • Oval, spherical , elongated	12		Hyaline Casts	• Tube/cylindrical shaped • Colorless • Smooth texture • Made of RBC

FIGURE 4. Distinguishing characteristics of urine sediment on the bases of their morphological structure.

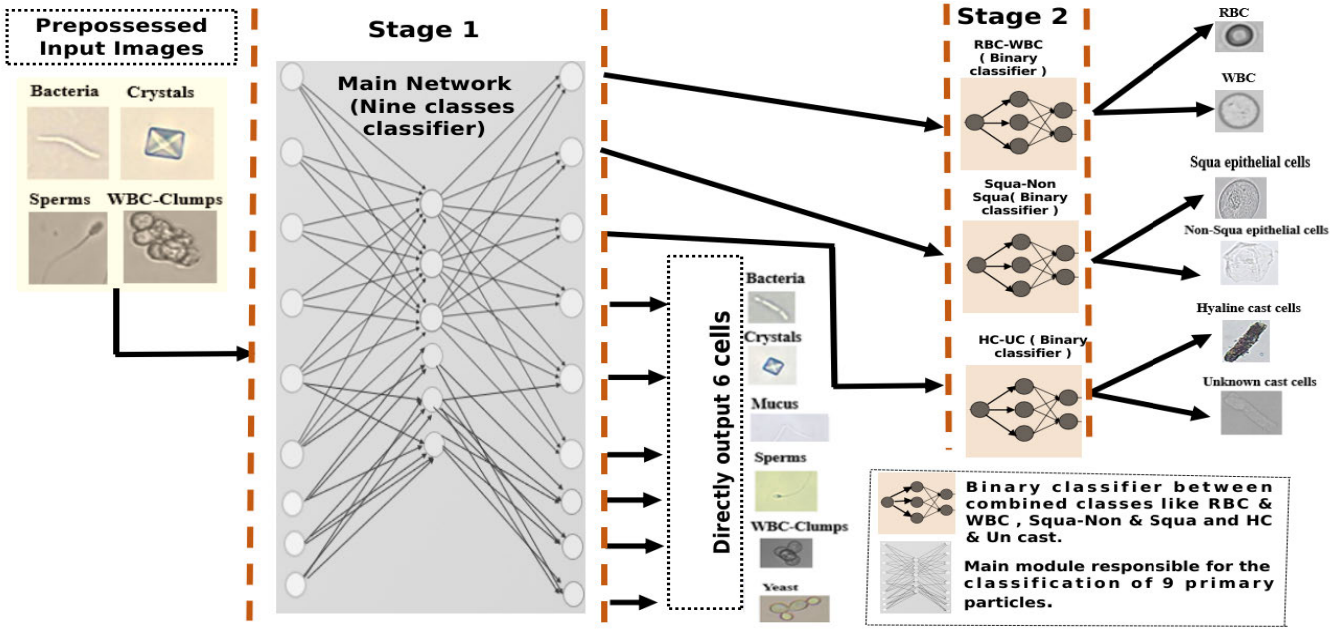

FIGURE 5. The complete process of the model for identifying structures in urine sediment images.

fine-tuning of architectures and hyperparameters contributes to the adaptability and effectiveness of the model in handling intricate classification scenarios.

IV. EXPERIMENTAL ANALYSIS

A. DATASET

In this section, we present a series of experimental results aimed at assessing the effectiveness of the proposed methodology. All experiments were executed on a computer system operating the Windows 10 OS (64-bit) with a 930GB hard disk, 8GB RAM, Intel(R) Core(TM) i7-6700 CPU (Processor), and Nvidia Tesla T4 GPU. The accuracy of a neural network is significantly contingent on the quality and quantity of the dataset employed for training. Hence, it is imperative to implement a robust data collection and labeling process.

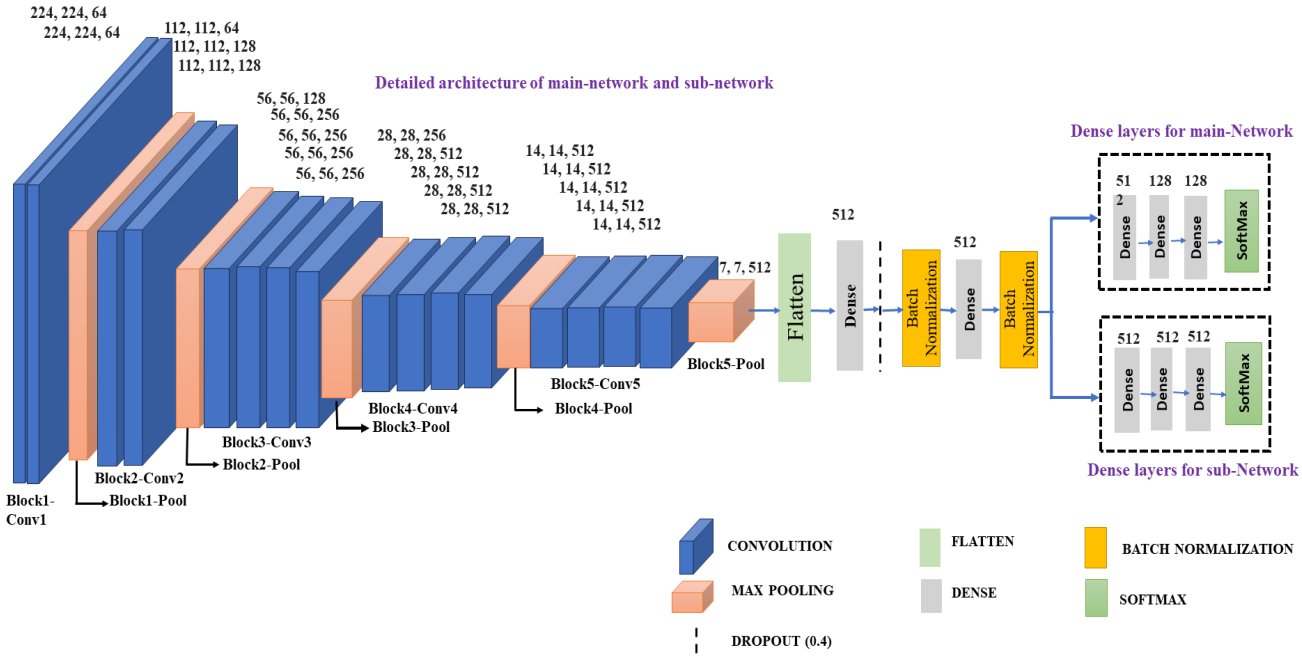

FIGURE 6. A detailed diagram of the improved VGG19 structure, highlighting both the main network and its sub-network.

FIGURE 7. Original image and six augmented variations for the sperm particle.

1) DATA COLLECTION PROCESS

To ensure the quality of the dataset, a substantial number of patient urine samples were collected from Bezmialem Vakif University Hospital in Turkey, employing a Dirui urine analyzer. This dataset was gathered between 2021 and 2022, with the comprehensive collection process spanning a duration of two months. The magnification factor for the Dirui urine analyzer was set at 20x, accurately reflecting the size relationship between particles in the images and their actual size in practice.

2) DATA LABELLING PROCESS

Following the data collection phase, medical professionals were engaged to meticulously label and verify the data, ensuring accuracy. High-resolution images were obtained from each sample and then segmented, with each segment containing a single particle. The labeling and verification process extended over a period of five months, resulting in a comprehensive dataset comprising 12 categories of urine sediment. These categories include Bacteria, RBC-WBC (subdivided into RBC and WBC), Sperms, Casts (further categorized into Hyaline Cast and Unknown Casts), Epithelial cells (divided into Squamous epithelial cells and Non-Squamous epithelial cells), Mucus, WBC-Clumps, Crystals, and Yeast. Each category was meticulously identified and labeled, enabling detailed analysis and recognition of different types of urine sediment. The dataset was divided into three subsets using a standard data partitioning technique. Specifically, 90% of the data were allocated for training the network, 5% for validation purposes, and the remaining 5% for testing the network's performance. This approach ensures a proper evaluation and optimization of the neural network model. Figure. 8 illustrates a set of labeled sample images, while Table. 4 provides the initial count of urine particles for each class. The table also outlines the count of augmented images generated to address class imbalance concerns.

B. RESULTS OF MODIFIED VGG19

The model was trained for 100 epochs, with a learning rate of 0.00001. To minimize the fluctuations in model accuracy and

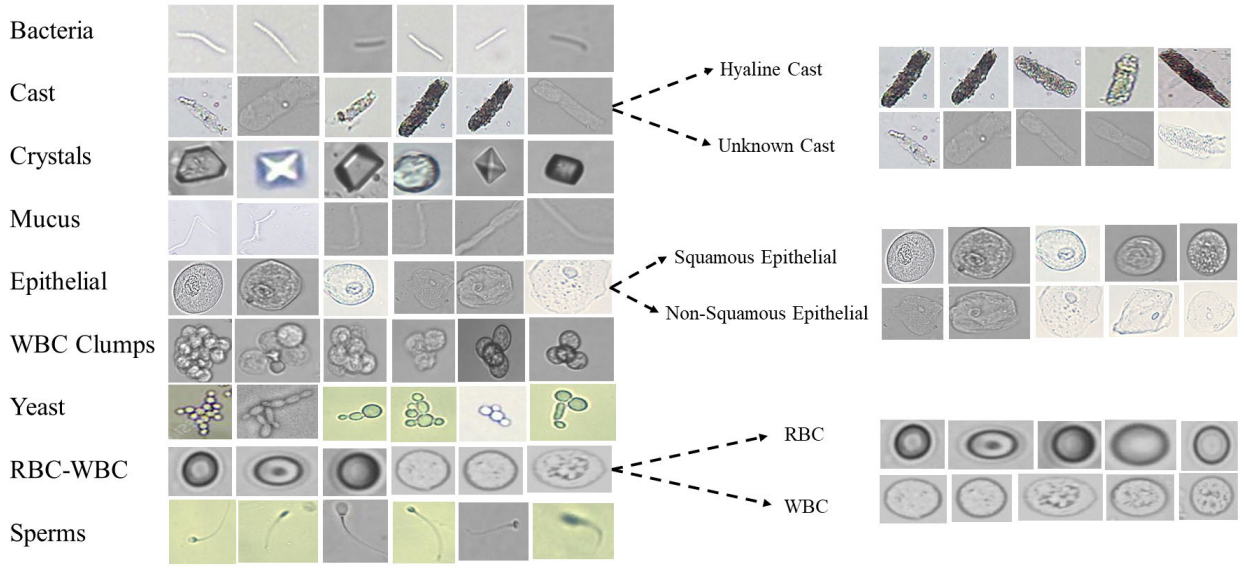

FIGURE 8. The dataset consists of urine sediment samples, with each category labeled and presented in the left column.

TABLE 4. Data-set details including original and augmented images count.

Sr #	Types of Urine Sediment	Number of Original Particles	Number of Augmented Images	Total Images
1	RBC	920	No augmentation	920
2	WBC	920	No augmentation	920
3	Crystals	920	No augmentation	920
4	Hyaline Cast	670	246	916
5	Unknown Cast	450	467	917
6	WBC Clumps	800	109	909
7	Squamous Epithelial Cells	912	No augmentation	912
8	Non-Squamous Epithelial Cells	400	518	918
9	Sperms	380	537	917
10	Yeast	850	68	918
11	Mucus	700	218	918
12	Bacteria	922	No augmentation	922
	Total	**8,844**		**Total = 11,007**

loss, hyperparameter tuning and architectural modifications were systematically executed.

Figure. 9 illustrates the impact of the changes through a comparison of the accuracy and loss curves. By adjusting hyperparameters and making architectural improvements, the model's performance became more stable and reliable, leading to smoother and more consistent accuracy and loss curves. The confusion matrix is represented in Figure. 10. While receiving operating curve and precision confidence curve are shown in Figure. 11. The curve illustrates the model's ability to correctly classify every instance belonging to each class, demonstrating a high level of precision and effectiveness. Additionally, the ROC curve displays 100% micro and macro averaging accuracy, which indicates the model's performance in making accurate predictions across all classes. This figure underscores the model's reliability and robustness, making it highly desirable for multi-class classification tasks. Macro-averaging and weighted-averaging are very useful measures to evaluate the performance of multi-category recognition models. Macro-averaging involves calculating individual index values for each category and then computing their arithmetic average across all categories. In a recognition task with n categories, the macro-average is estimated as:

$$\text{MacroF} = \frac{2 \times \text{MacroP} \times \text{MacroR}}{\text{MacroP} + \text{MacroR}} \tag{1}$$

where

$$\text{MacroP} = \frac{1}{n}\sum_{i=1}^{n} P_i \tag{2}$$

$$\text{MacroR} = \frac{1}{n}\sum_{i=1}^{n} R_i \tag{3}$$

where P is the precision and it is defined as

$$P = \frac{TP}{TP + FP} \tag{4}$$

and R is the recall rate, which is often referred to as sensitivity. It is an important metric for assessing the effectiveness of

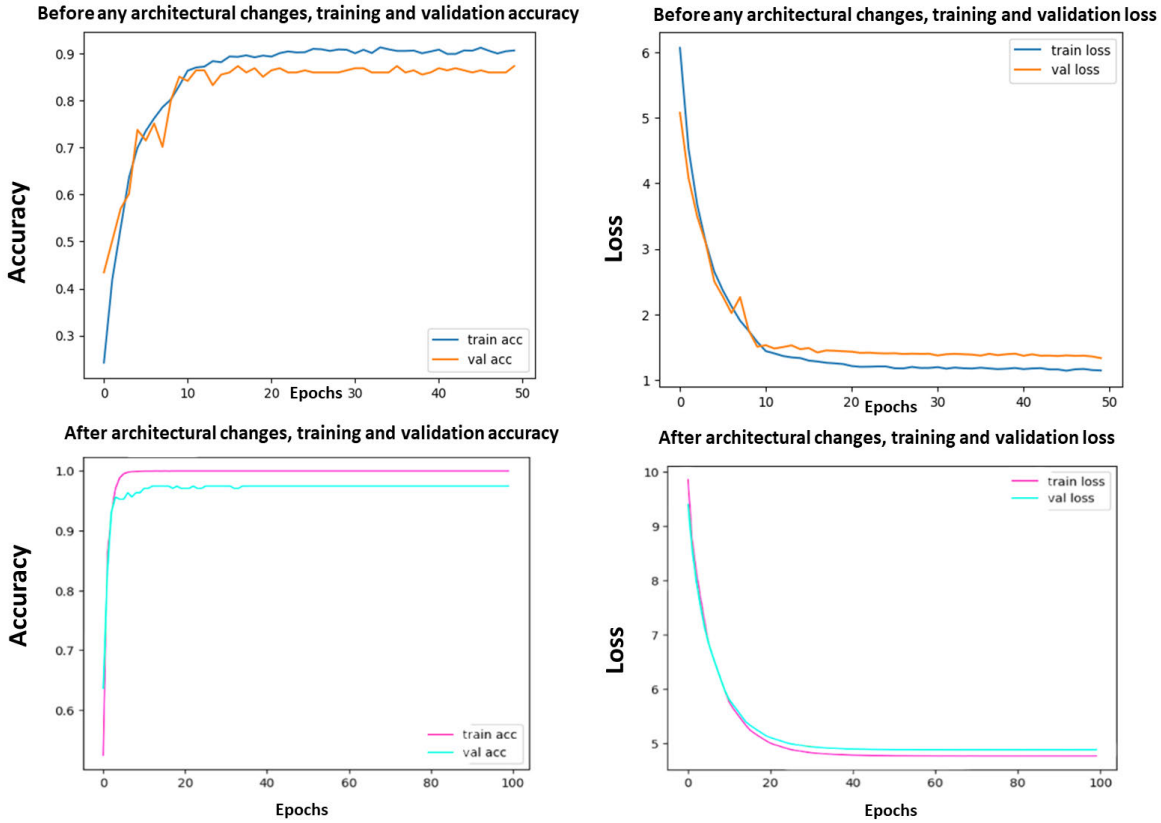

FIGURE 9. Comparison of accuracy and loss curves before and after implementing architectural changes in the modified VGG19 model. Top row depict the curves before architectural changes, while the bottom row illustrate accuracy and loss curves after implementing architectural changes.

recognition tasks, defined as follows:

$$\text{Sensitivity} = \frac{\text{TP}}{\text{TP} + \text{FN}} \tag{5}$$

Here, ''TP'' denotes true positives, which refers to the number of correctly identified positive instances, ''FP'' represents false positives, which is the number of incorrectly identified positive instances and ''FN'' denotes false negatives, which represents the number of incorrectly identified negative instances. In table 3, the performance evaluation metrics are presented for the nine-class classification. The weighted average is calculated for each metric by summing the index value multiplied by a specific weighted term assigned to each class.

$$\text{Weighted Average} = \sum_{i=1}^{n} w_i \times \text{Index value for category } i \tag{6}$$

In Figure. 12, the predictive performance of the model is presented, when it is tested on a dataset containing nine distinct categories. The model demonstrates impressive performance, both in terms of accuracy and computational time. As for computational performance, it achieves an inference time of only 61 ms per image. The overall average

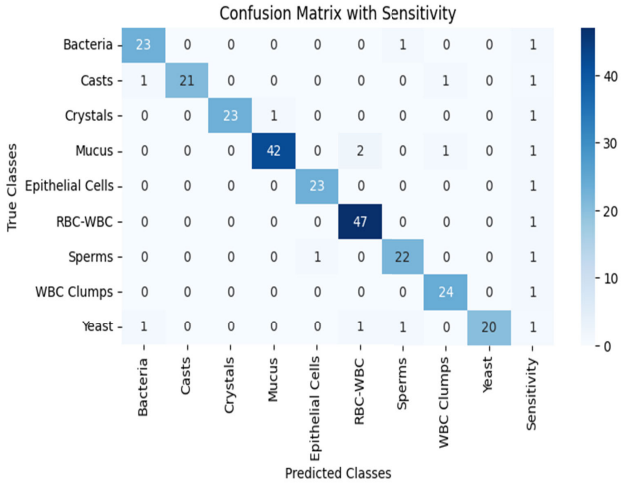

FIGURE 10. Confusion Matrix for test set using modified VGG19 for nine classes.

precision across these categories is 35%. The RBC-WBC category stands out with the highest average precision of 49%, making it the top-performing category in terms of

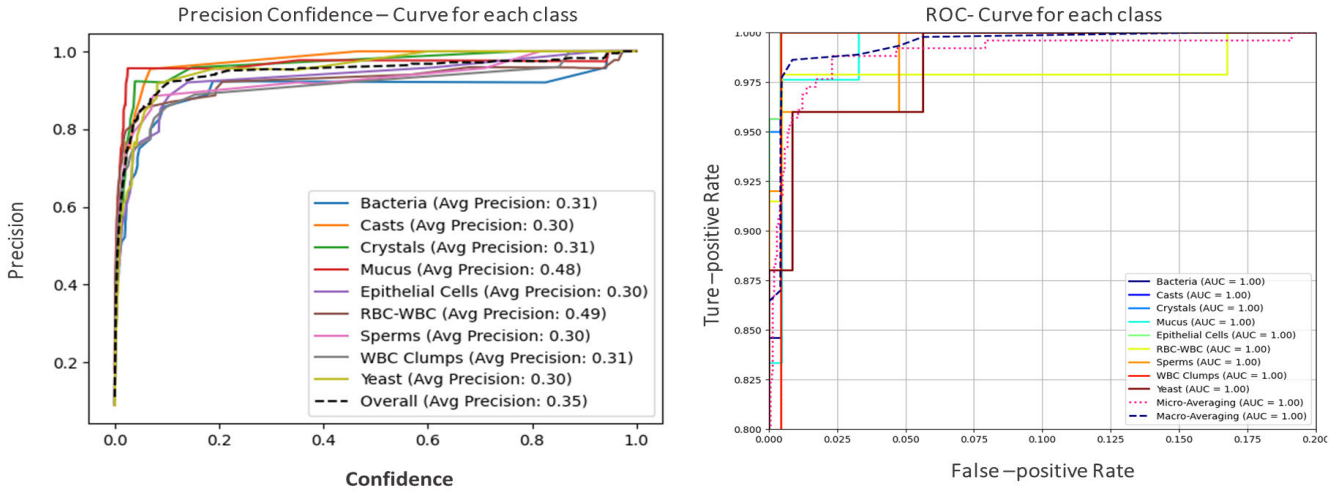

FIGURE 11. ROC curves and precision-confidence curves for the modified VGG19 model across nine categories.

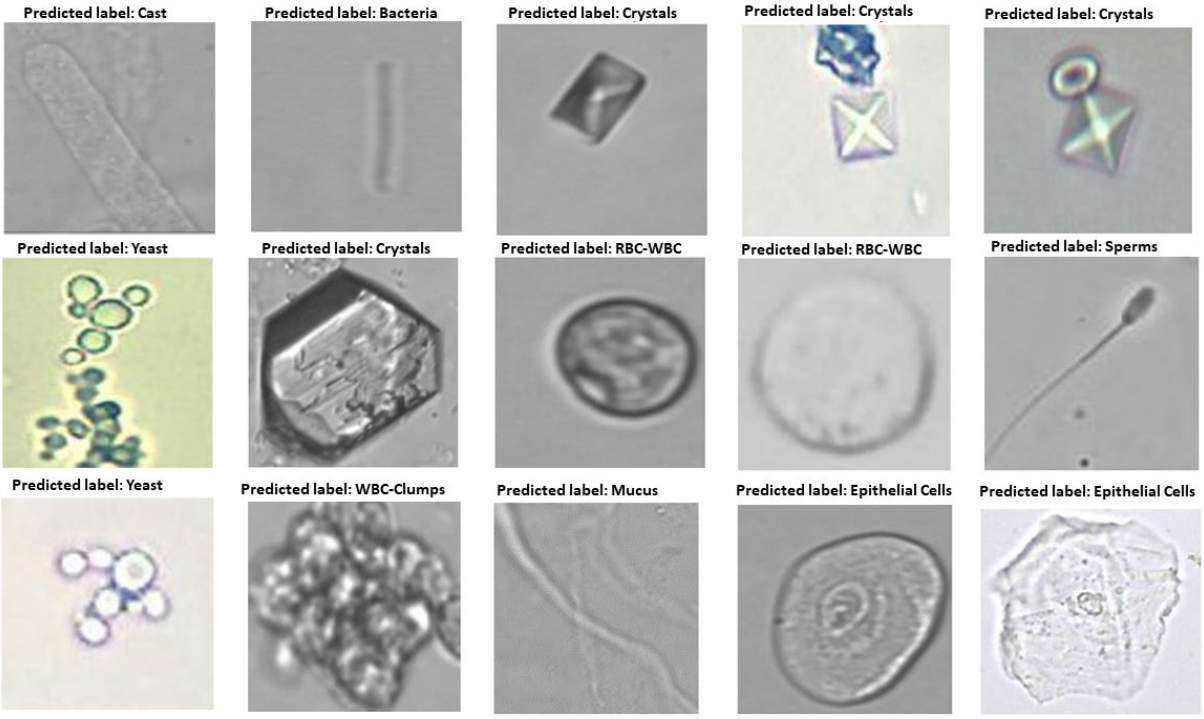

FIGURE 12. Prediction results of the modified VGG19 for 9 classes.

precision. Similarly, the Mucus category achieved the second-highest precision among all the categories. The proposed method exhibits clear advantages compared to state-of-the-art, as illustrated in Table 5. It can be seen that the proposed method's accuracy is a little lower [3]; however, it exceeds [4], [5], [18], [45], and [44]. It is worth noting that the methodologies proposed in [3] can successfully handle only 7 out of the 12 categories in the given recognition challenge. In contrast, the method proposed in this work covers most of the categories, and can robustly solve more complex and challenging recognition tasks as compared to previous methods. Consequently, It can be more useful in clinical settings. On a different note, even though the accuracy of the method described in [18] is lower, however, it encompasses a broader range of urine sediments. The focus of the current research is on the diversity of urine sediments, even though the proposed method in [18] also take sub-types of yeast and crystals into account. All of those subtypes

TABLE 5. Comparison of accuracy and average time consumption among methods from different papers.

Sr#	Year	Techniques	Categories	Accuracy	Inference Time (ms)
1	2023	ACM mixer & DenseNet201 [3]	7 Types	98.52%	Not mentioned
2	2019	Combination of CNN with area feature algorithm [4]	10 Types	96.75%	61
3	2023	Resnet50 + LBP + mRMR + SVM [5]	8 Types	96%	Not mentioned
4	2023	US-RepNet [18]	16 (subtypes of crystals)	94%	Not mentioned
5	2023	Swin-LBP [44]	7 Types	92.60%	Not mentioned
6	2020	LeNet-5 neural network [45]	4 Types	94.29%	Not mentioned
7	2023	Proposed Method	12 Types	98%	61

belonged to either crystal or yeast particles. The performance improvement in the proposed method can be attributed to following factors.

- The proposed method employs a data-centric approach, collaborating with experts to tackle class imbalance, missing data, and labeling inaccuracies. This ensures the availability of accurate and high-quality data, leading to reliable model decisions and improved predictions.
- we used a cascaded approach consisting of four modified versions of CNNs based on VGG19 architecture, which make use of transfer learning and augmentation techniques to enhance overall performance. The introduction of sub-modules has played a critical role in resolving confusion between categories which, otherwise, looked similar, thereby resulting in improved recognition capabilities.
- The uneven distribution of urine sediment particles led to variations in identified particles among different samples. To address this issue and optimize computing resources, a pre-processing step is used to segment micro-images into smaller images, each with a unique label. This has resulted in faster particle traversal, convolution, and classification.

The main classifier shows an average recognition time of 61 milliseconds, which is consistent with the findings of the study by [4]. Furthermore, the proposed approach has proved to be more efficient in handling a broader range of sediment classes compared to alternative methods such as [3], [4], [5], and [44].

1) RESULTS OF OTHER SUB-MODULES

Due to morphological similarities, it is hard to distinguish between RBCs, WBCs, Squamous Epithelial Cells, Non-Squamous Epithelial Cells, hyaline casts, and unknown Casts. To tackle this challenge, dedicated sub-modules have been incorporated for sub-class recognition. These sub-modules consist of the RBC-WBC classifier, Squa Non-Squa classifier, and HC-UC classifier. Their primary function is to efficiently differentiate between these particles, addressing the problem of misclassification.

TABLE 6. Test Classification Report for the test set using modified VGG19.

Class	Precision	Recall	F1-score
Bacteria	0.86	1.00	0.92
Casts	1.00	0.96	0.98
Crystals	1.00	0.96	0.98
Mucus	1.00	1.00	1.00
Epithelial Cells	0.96	1.00	0.98
RBC-WBC	1.00	1.00	1.00
Sperms	0.95	0.90	0.92
WBC Clumps	1.00	1.00	1.00
Yeast	1.00	0.92	0.96
Accuracy	0.98		
Macro avg	0.97	0.97	0.97
Weighted avg	0.98	0.98	0.98

The incorporation of additional training iterations elevated the comprehensive process of categorizing urine sediment in its analysis, resulting in increased precision and reliability in identification of diverse particles. The classification results for the individual sub-classifiers are presented in Table. 7 Table. 8 and Table. 9, demonstrating substantial weighted average accuracies of 98%, 96%, and 97%, respectively. Furthermore, the system's inference time per image was observed to be a swift 61 milliseconds. Figure. 13, Figure. 15, and Figure. 17 illustrate the curves, displaying accuracy during training and validation, along with the loss, for all sub-modules. These graphical representations provide insights into the shifts in accuracy and loss as the model undergoes training and validation. This provides a comprehensive understanding of the model's performance and its generalization capability to the dataset.

Furthermore, Figure. 14, Figure. 16, and Figure. 18 present precision-confidence curves and ROC curves, highlighting average precisions of 84% across all sub-modules. Specifically, examining the ROC curve for the RBC-WBC classifier reveals an outstanding accuracy of 99% for every

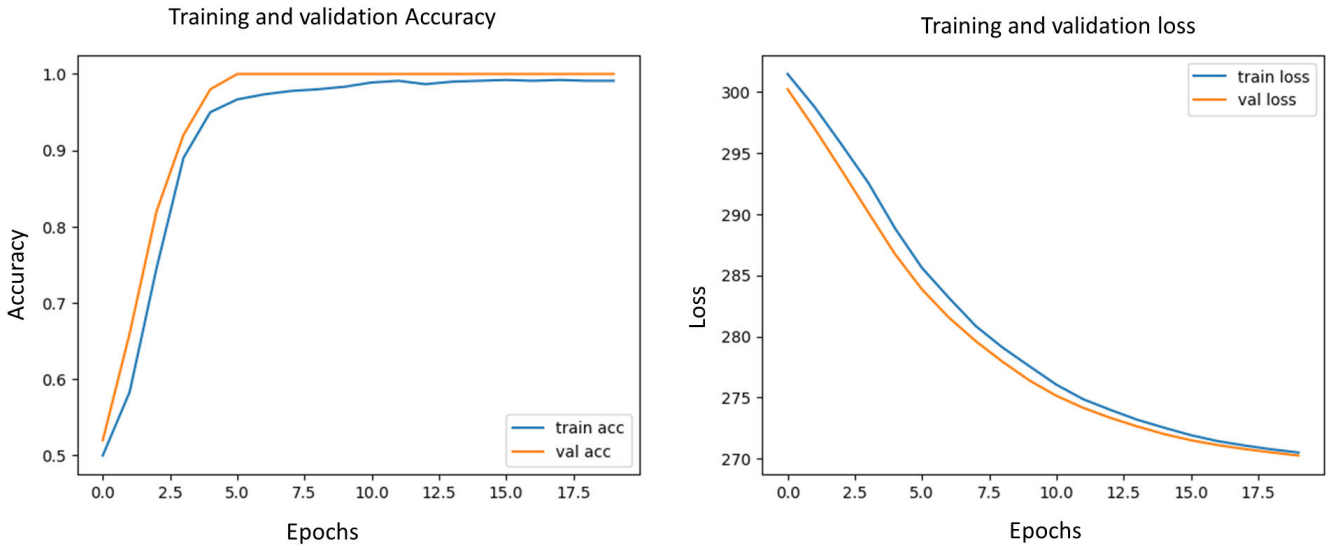

FIGURE 13. Graphs illustrating the training and validation accuracy as well as the loss of the RBC-WBC Classifier.

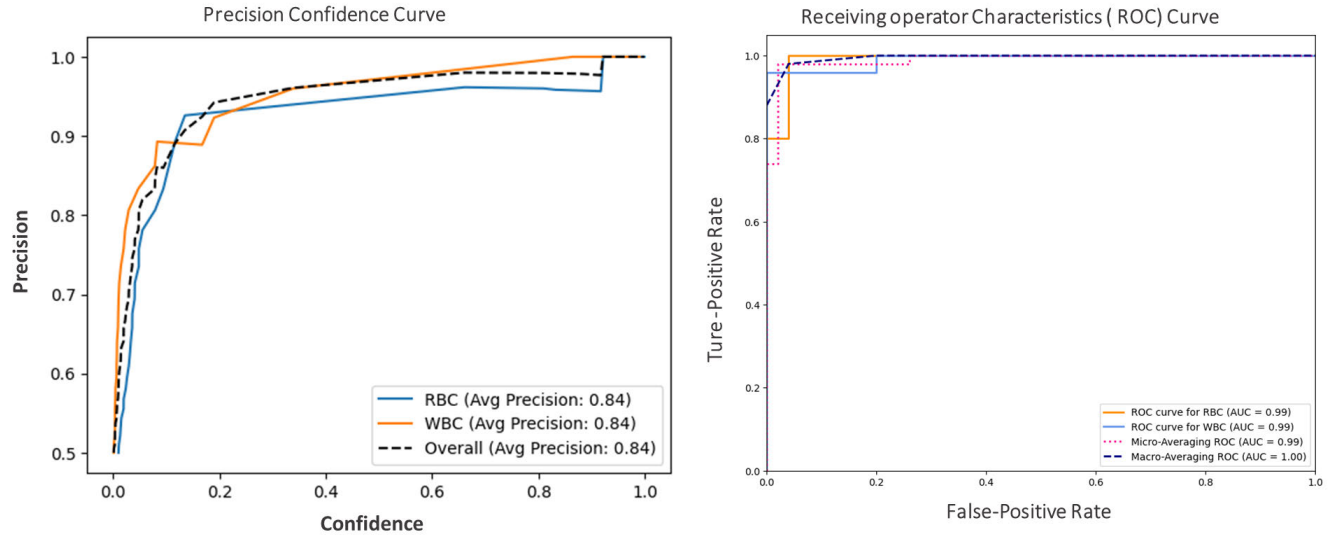

FIGURE 14. The precision-confidence curve and ROC curve for the RBC-WBC classifier.

TABLE 7. Test classification report for the test set of RBC-WBC classifier.

Class	Precision	Recall	F1-score
RBC	0.96	1.00	0.98
WBC	1.00	0.96	0.98
Accuracy	0.98		
Macro avg	0.98	0.98	0.98
Weighted avg	0.98	0.98	0.98

particle, with equally impressive micro and macro averaging accuracies of 99% and 100%, respectively. This performance underscores its accuracy in correctly classifying red and white blood cells. Similarly, the Squa Non-Squa classifier demonstrates consistency with both micro and macro averaging accuracies, affirming its reliability in distinguishing between "Squa" and "Non-Squa" categories. The HC-UC classifier demonstrates 98% accuracy for each particle, along with 99% mark for macro and micro-averaging accuracies, demonstrating its capability to differentiate between "HC" and "UC" categories. In summary, all binary classifiers demonstrate robust performance, characterized by elevated precision and reliability in their distinct classifications.

Figure. 20 displays the confusion matrix for the sub-modules. The confusion matrix summarizes the number of correct and incorrect predictions made by each sub-module,

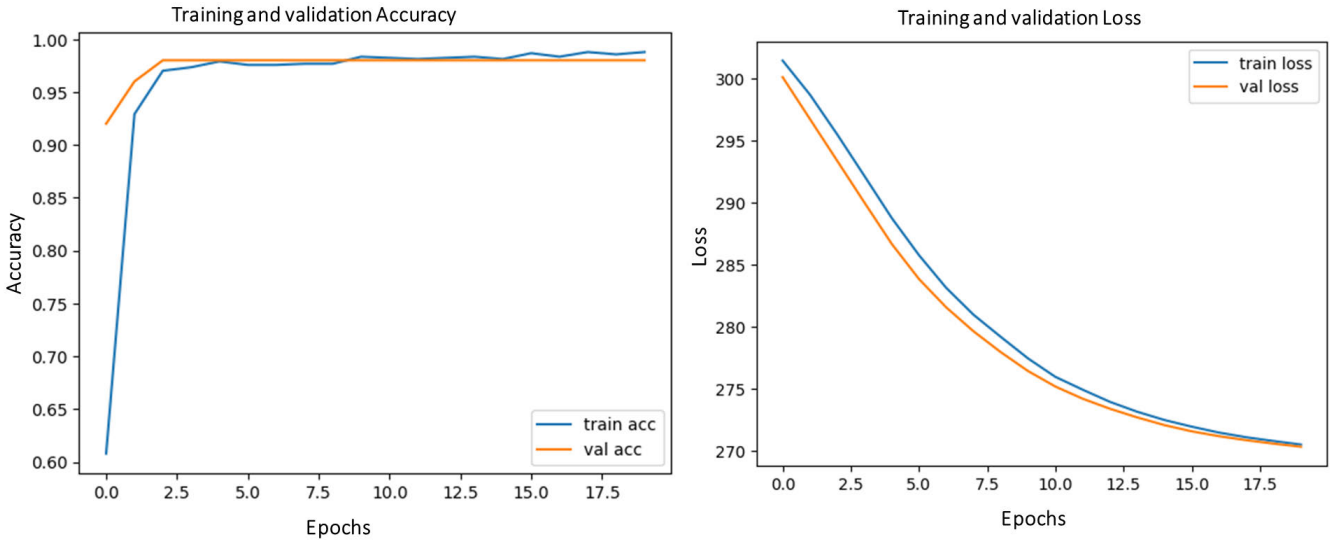

FIGURE 15. Curves depicting the training and validation accuracy and loss of the Squa-Non Squa classifier.

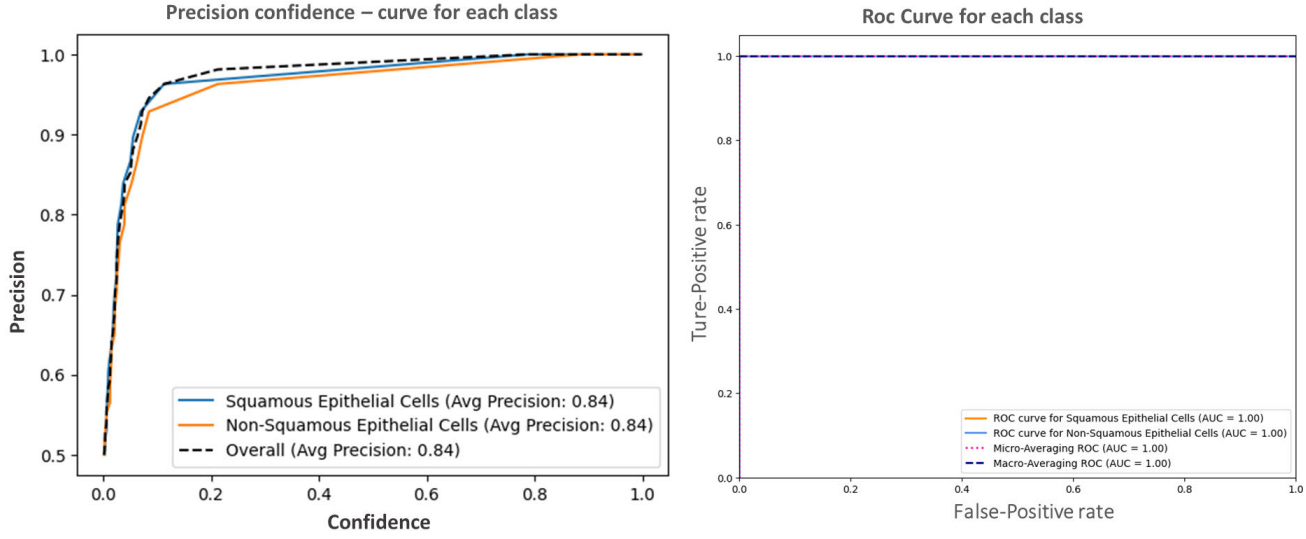

FIGURE 16. The precision-confidence curve and ROC curve for the Squa-Non Squa classifier.

TABLE 8. Test classification report for the test set of Squa-Non Squa classifier.

Class	Precision	Recall	F1-score
Squamous Epithelial	0.93	1.00	0.96
Non-Squamous Epithelial	1.00	0.92	0.96
Accuracy	0.96		
Macro avg	0.96	0.96	0.96
Weighted avg	0.96	0.96	0.96

TABLE 9. Test classification report for the test set of HC-UC classifier.

Class	Precision	Recall	F1-score
Hyaline Cast	1.00	0.92	0.96
Unknown Cast	0.93	1.00	0.97
Accuracy	0.96		
Macro avg	0.97	0.96	0.96
Weighted avg	0.97	0.96	0.96

offering valuable insights into the model's performance in distinguishing between different particle categories. On the other hand, Figure. 19 showcases the prediction results obtained from all three sub-modules.

V. DISCUSSION

The proposed innovative approach for automated urine sediment analysis represents a significant advancement in the realm of medical image processing. By synergizing

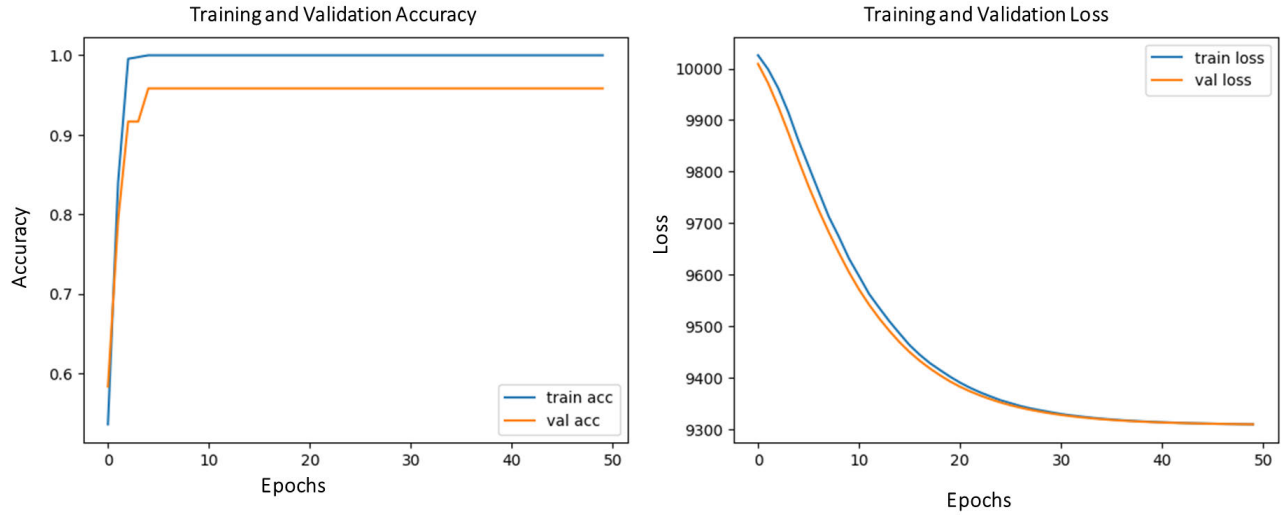

FIGURE 17. Curves illustrating the accuracy and loss during training and validation of the HC-UC classifierr.

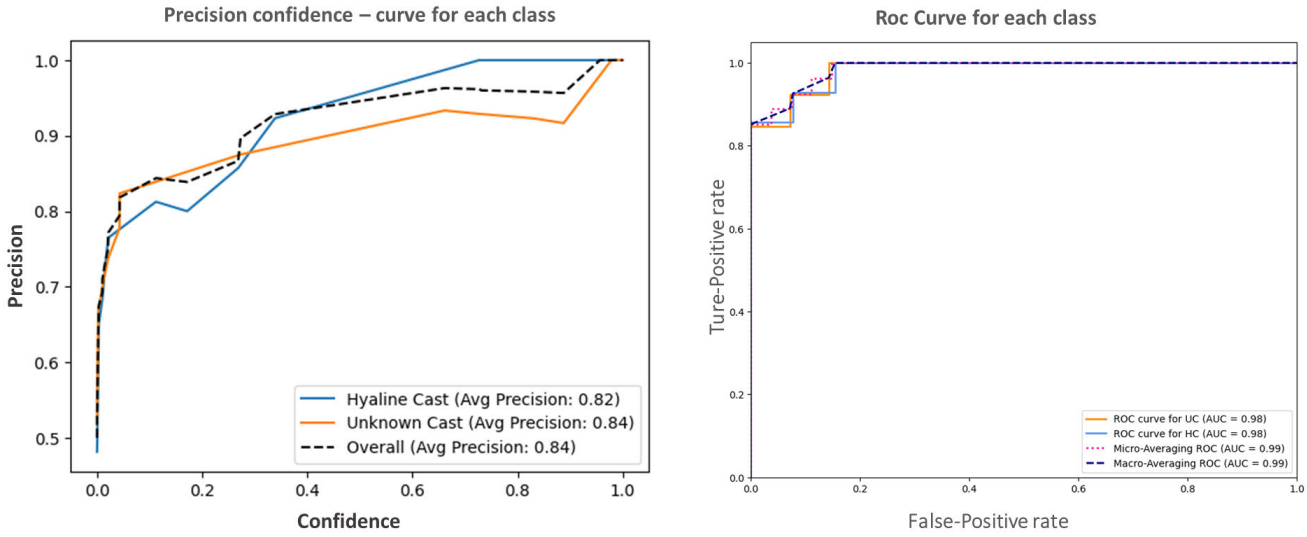

FIGURE 18. The precision-confidence curve and ROC curve for the HC-UC classifier.

data-centric and model-centric methods, it effectively addresses several critical challenges that have impeded the development of accurate and efficient automated analyzers. A key strength of the proposed method lies in its adept handling of missing data and effective resolution of class imbalance. In contrast, previous research [5], [44] has underscored that grappling with missing data and class imbalance could introduce biases and potentially result in low recognition performance. The proficient management of missing data is a notable achievement facilitated through the utilization of the proposed data-centric approach. The incorporation of the modified VGG19 model played a pivotal role in enhancing the recognition performance, particularly for categories prone to confusion in urine sediment images. Conventional image processing methods encountered difficulties in recognizing large-scale categories in urine sediment images, leading to confusion. However, the strategic implementation of the VGG19 model enabled us to achieve high levels of computational efficiency and accuracy. This success allowed for the successful identification of 12 distinct categories of urine sediment images, effectively overcoming and resolving the category confusion issue highlighted in prior research [3], [5], [18], [44]. The extensive training dataset, comprising 11,000 urine sediment images, empowered the proposed model to attain an impressive test accuracy of 98%. This outcome demonstrates the model's robust ability to generalize to unseen data, rendering it highly reliable and suitable for real-world applications in medical diagnostics. Furthermore, the inference time of 61ms per image showcases the practicality and time-saving nature of

FIGURE 19. Prediction results of all three sub classifiers.

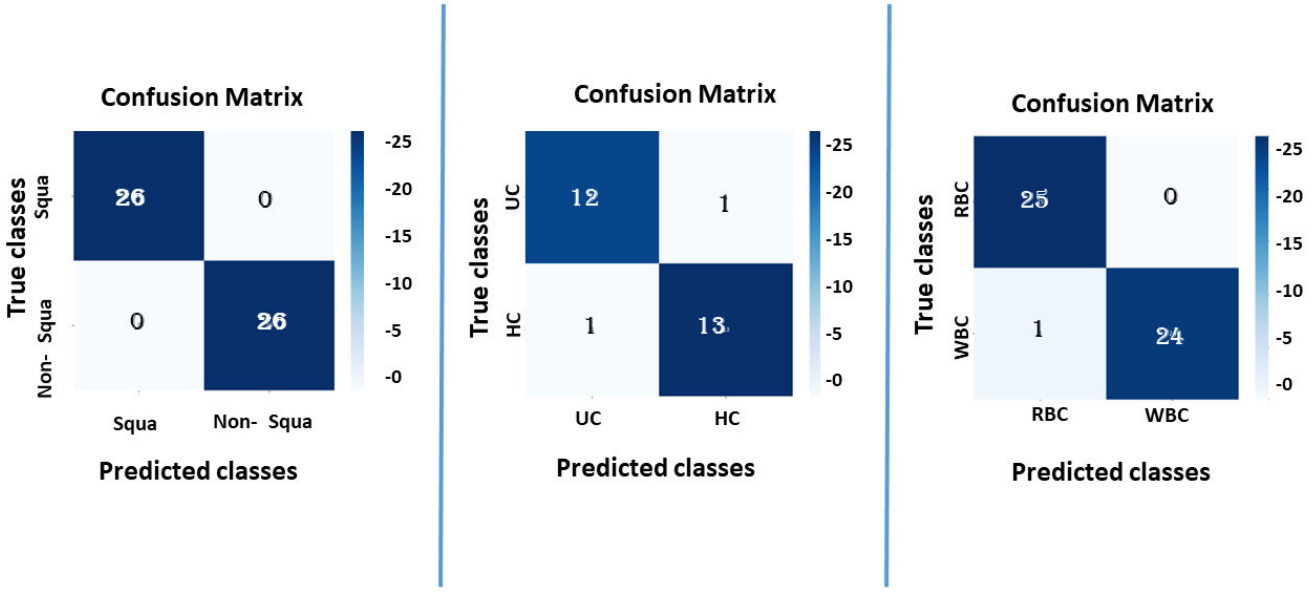

FIGURE 20. Conusion matrix for all three sub classifiers.

the proposed approach. This rapid inference time makes it feasible to analyze a large number of urine sediment samples within a short period, thereby enhancing the efficiency of medical laboratories and reducing the burden on healthcare professionals. Last but not least, the use of Convolutional Neural Networks (CNN) as the underlying architecture opens up avenues for further research. This adaptability renders the proposed approach responsive to evolving medical requirements and advancements, paving the way for further innovations in the field.

A. ABLATION STUDY

A comprehensive set of ablations was conducted to highlight the classification performance achieved by the proposed

modified-VGG19 model. In the first phase, the performance of the proposed model was compared with seven distinct CNN architectures for a thorough analysis. Subsequently, the outcomes were compared amongst VGG19 models, both before and after applying modifications, under different conditions. These specific scenarios are detailed below.

- **Comparison of Seven CNN Architectures:** Seven distinct CNN architectures, including AlexNet, ResNet101, VGG16, InceptionV3, MobileNet, ResNet50, and VGG19, were evaluated. Among these, VGG19 demonstrated the highest accuracy with good prediction results.
- **Experiments with VGG19:** A series of experiments were conducted with VGG19. Initially, VGG19 was implemented using original images without data augmentation. Subsequently, the experiments were repeated with data augmentation, followed by incorporating transfer learning. Finally, modifications were introduced to the VGG19 architecture, and experiments were conducted with augmentation and transfer learning, achieving the highest accuracy in this configuration.

The results of this ablation study are illustrated in Figure. 21 and Figure. 22. As shown in Figure. 21,the proposed modified VGG19 model accomplished the highest accuracy of 98% when applied to the dataset, confirming its compatibility with the given data. All CNN architectures underwent evaluation with augmentation and transfer learning on the dataset. While MobileNet also achieved an accuracy of 97% Figure. 22 reveals that the proposed modified-VGG19 model achieved the highest accuracy. A number of experiments with varying configurations have been conducted. Initially, the baseline VGG19 was implemented on the original unbalanced dataset, where some of the classes lacked sufficient images, as detailed in Table 4. The obtained accuracy was 88.6%, indicating generally accurate predictions, but with a noticeable tendency towards overfitting. Subsequently, different augmentation techniques were applied to address the imbalance in the data, resulting in a 4.1% increase in accuracy. The utilization of transfer learning significantly impacted model accuracy; however, overfitting persisted. In the final phase, VGG19 went through architectural adjustments and fine-tuning, as outlined in Section III-C. Despite a modest 1% increase in accuracy after modification, this adjustment proved beneficial in terms of mitigating prediction errors. Notably, the model successfully alleviated fluctuations in training and validation curves, vouching for improved stability.

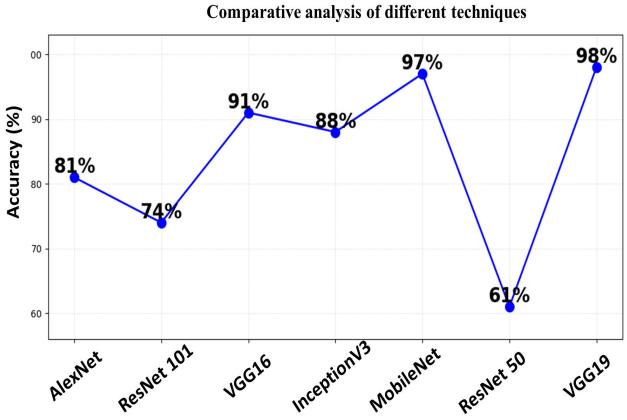

FIGURE 21. Comparing the accuracy scores of various CNN architectures.

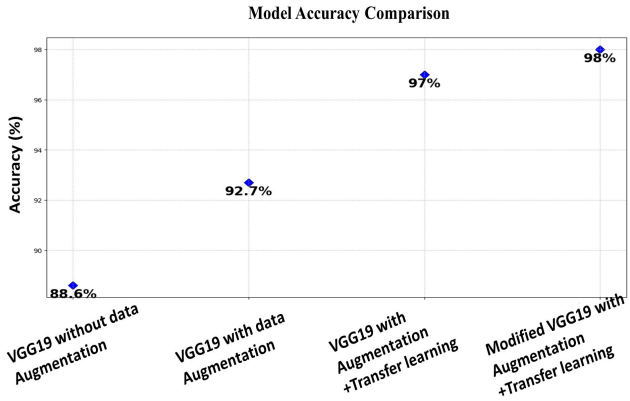

FIGURE 22. Ablation study of 4 experiments.

B. LIMITATIONS

In urine sediment analysis, one of the common limitations is the recognition of all possible sediment particle classes and their sub-classes. Broadly, they can be categorized into 10 main classes, with 27 sub-classes, as illustrated in Figure 1. In this work, the proposed method successfully classifies 9 main categories and 6 subcategories, with a total of 12 classes. The number of classes is limited due to constraints in the availability of required data. This limitation could be alleviated by incorporating more labeled data. Another prevalent issue is the class imbalance in urine sediment data. In most urine datasets, the count for some class particles is significantly higher than others; for example, RBC and WBC clumps are generally higher in numbers than other particles. To mitigate this issue, data augmentation techniques have been applied. This data augmentation positively affects the model's accuracy and can further address the class imbalance problem by increasing the data samples to achieve a more balanced distribution of original images across all classes. On the other hand, the resizing mechanism employed by Convolutional Neural Networks (CNNs) can potentially diminish or erase the distinctive size characteristics of cells, leading to a loss of information related to cell sizes. Furthermore, CNN models demand a substantial amount of labeled data to attain a high classification rate. In the future, alternative deep learning models, such as transformers, can be employed to achieve high accuracy with a reduced need for labeled data.

VI. CONCLUSION

Urine sediment tests are crucial for diagnosing abnormal diseases related to the urinary tract by identifying key cellular components in urine samples, such as red blood cells and white blood cells. Manual urinalysis using human

eyes is subjective, time-consuming, and prone to errors, necessitating the development of image processing methods for automated analysis. Automated urine analyzers enhance patient care and overall performance in smart healthcare by enabling real-time data transmission and analysis. This paper presented a significant advancement in automated urine sediment analysis by proposing a combination of data-centric and model-centric approaches. The incorporation of a modified VGG19 deep learning model further improved recognition performance, especially for challenging categories with similar features. To achieve the research goal, urine data was collected and categorized with insights from medical experts due to the limited availability of public data with large categories. Through the utilization of an 11,000-image urine sediment training dataset, the model demonstrated efficiency in precisely classifying 12 urine sediment image categories. The achieved accuracy of 98% on the test set, along with an inference time of 61ms per image, underscores the effectiveness and practicality of the proposed approach. The methodology not only addresses challenges related to data acquisitions, labeling, missing data, and class imbalance but also streamlines the recognition process for large-scale categories. Furthermore, the CNN exhibits robust capability for further enhancement, allowing for the incorporation of additional sub-categories in real-world applications.

VII. FUTURE WORK

Future work for this research involves broadening its scope to include a broader range of subcategories within the 12 categories of urine particles. Additionally, exploring new techniques to address the imbalanced distribution of images across classes offers a promising avenue for further research. Towards this end, additional classes can be labeled for subcategory classification, specifically targeting those particles that rarely appear in urine sediment images. Such an approach can further address the class imbalance issue, potentially contributing to the development of more robust automated urine sediment analyzers in clinical settings.

ACKNOWLEDGMENT

This Research is funded by Researchers Supporting Project Number (RSPD2024R947), King Saud University, Riyadh, Saudi Arabia. The authors also want to acknowledge the support of The Scientific and Technological Research Council of Türkiye (TÜBİTAK) to conduct this research, under project number: 220N334.

REFERENCES

[1] F. Hao, X. Li, M. Li, Y. Wu, and W. Zheng, "An accurate urine red blood cell detection method based on multi-focus video fusion and deep learning with application to diabetic nephropathy diagnosis," *Electronics*, vol. 11, no. 24, p. 4176, Dec. 2022.

[2] C. C. Hortinela, J. R. Balbin, J. C. Fausto, and K. K. Viray, "Identification of crystals present in a urine sediment based on adaptive boosting algorithm," in *Proc. IEEE 11th Int. Conf. Humanoid, Nanotechnol., Inf. Technol., Commun. Control, Environ., Manag.*, Nov. 2019, pp. 1–4.

[3] M. Erten, I. Tuncer, P. D. Barua, K. Yildirim, S. Dogan, T. Tuncer, R.-S. Tan, H. Fujita, and U. R. Acharya, "Automated urine cell image classification model using chaotic mixer deep feature extraction," *J. Digit. Imag.*, vol. 36, no. 4, pp. 1675–1686, May 2023.

[4] Q. Ji, X. Li, Z. Qu, and C. Dai, "Research on urine sediment images recognition based on deep learning," *IEEE Access*, vol. 7, pp. 166711–166720, 2019.

[5] M. Yildirim, H. Bingol, E. Cengil, S. Aslan, and M. Baykara, "Automatic classification of particles in the urine sediment test with the developed artificial intelligence-based hybrid model," *Diagnostics*, vol. 13, no. 7, p. 1299, Mar. 2023.

[6] G. L. Streun, A. E. Steuer, L. C. Ebert, A. Dobay, and T. Kraemer, "Interpretable machine learning model to detect chemically adulterated urine samples analyzed by high resolution mass spectrometry," *Clin. Chem. Lab. Med. (CCLM)*, vol. 59, no. 8, pp. 1392–1399, Jul. 2021.

[7] Q. Li et al., "Multi-class analysis of urinary particles based on deep learning," *Authorea Preprints*, pp. 1–14, 2020, doi: 10.22541/au.157878399.96593318.

[8] Q. Li, Z. Yu, T. Qi, L. Zheng, S. Qi, Z. He, S. Li, and H. Guan, "Inspection of visible components in urine based on deep learning," *Med. Phys.*, vol. 47, no. 7, pp. 2937–2949, Jul. 2020.

[9] B. Zeb, A. Khan, Y. Khan, M. F. Masood, I. Tahir, and M. Asad, "Towards the selection of the best machine learning techniques and methods for urinalysis," in *Proc. 12th Int. Conf. Mach. Learn. Comput.*, Feb. 2020, pp. 127–133.

[10] K. Suhail and D. Brindha, "A review on various methods for recognition of urine particles using digital microscopic images of urine sediments," *Biomed. Signal Process. Control*, vol. 68, Jul. 2021, Art. no. 102806.

[11] Q. Wang, Q. Sun, and Y. Wang, "A two-stage urine sediment detection method," *Proc. SPIE*, vol. 11584, pp. 15–21, Nov. 2020.

[12] C. Li, Y. Y. Tang, H. Luo, and X. Zheng, "Join Gabor and scattering transform for urine sediment particle texture analysis," in *Proc. IEEE 2nd Int. Conf. Cybern. (CYBCONF)*, Jun. 2015, pp. 410–415.

[13] Z. Chen et al., "An efficient particle YOLO detector for urine sediment detection," in *Proc. Int. Conf. Mach. Learn. Cyber Secur.* Cham, Switzerland: Springer, 2022, pp. 294–308.

[14] G. Litjens, T. Kooi, B. E. Bejnordi, A. A. A. Setio, F. Ciompi, M. Ghafoorian, J. A. Van Der Laak, B. Van Ginneken, and C. I. Sánchez, "A survey on deep learning in medical image analysis," *Med. Image Anal.*, vol. 42, pp. 60–88, Dec. 2017.

[15] Y. LeCun, Y. Bengio, and G. Hinton, "Deep learning," *Nature*, vol. 521, no. 7553, pp. 436–444, 2015.

[16] Z. M. Khalid, R. Scddeek Hawezi, and S. R. Muhamad Amin, "Urine sediment analysis by using convolution neural network," in *Proc. 8th Int. Eng. Conf. Sustain. Technol. Develop. (IEC)*, Feb. 2022, pp. 173–178.

[17] K. P. Aglibot, J. A. Angeles, J. F. Gecana, A. B. Germano, J. A. Macalindong, and R. E. Tolentino, "Urine crystal classification using convolutional neural networks," in *Proc. Int. Visualizat., Informat. Technol. Conf. (IVIT)*, Nov. 2022, pp. 245–250.

[18] Q. Ji, Y. Jiang, Z. Wu, Q. Liu, and L. Qu, "An image recognition method for urine sediment based on semi-supervised learning," *IRBM*, vol. 44, no. 2, Apr. 2023, Art. no. 100739.

[19] H. Atici, H. E. Kocer, A. Sivrikaya, and M. Dagli, "Analysis of urine sediment images for detection and classification of cells," *Sakarya Univ. J. Comput. Inf. Sci.*, vol. 6, no. 1, pp. 37–47, Apr. 2023.

[20] R. Awan, K. Benes, A. Azam, T. Song, M. Shaban, C. Verrill, Y. W. Tsang, D. Snead, F. Minhas, and N. Rajpoot, "Deep learning based digital cell profiles for risk stratification of urine cytology images," *Cytometry A*, vol. 99, no. 7, pp. 732–742, Jul. 2021.

[21] O. Ronneberger, P. Fischer, and T. Brox, "U-Net: Convolutional networks for biomedical image segmentation," in *Proc. Int. Conf. Med. Image Comput. Comput.-Assist. Intervent.* Cham, Switzerland: Springer, 2015, pp. 234–241.

[22] Y. Liang, Z. Tang, M. Yan, and J. Liu, "Object detection based on deep learning for urine sediment examination," *Biocybernetics Biomed. Eng.*, vol. 38, no. 3, pp. 661–670, 2018.

[23] S. Akhtar, M. Hanif, and H. Malih, "Automatic urine sediment detection and classification based on YOLOv8," in *Proc. Int. Conf. Comput. Sci. Appl.* Cham, Switzerland: Springer, 2023, pp. 269–279.

[24] M. Badawy, A. M. Almars, H. M. Balaha, M. Shehata, M. Qaraad, and M. Elhosseini, "A two-stage renal disease classification based on transfer learning with hyperparameters optimization," *Frontiers Med.*, vol. 10, Apr. 2023, Art. no. 1106717.

[25] K. S. Lee, H. J. Lim, K. Kim, Y.-G. Park, J.-W. Yoo, and D. Yong, "Rapid bacterial detection in urine using laser scattering and deep learning analysis," *Microbiol. Spectr.*, vol. 10, no. 2, Apr. 2022, Art. no. e01769.
[26] X. Zhang, L. Jiang, D. Yang, J. Yan, and X. Lu, "Urine sediment recognition method based on multi-view deep residual learning in microscopic image," *J. Med. Syst.*, vol. 43, no. 11, pp. 1–10, Nov. 2019.
[27] J. S. Velasco, M. K. Cabatuan, and E. P. Dadios, "Urine sediment classification using deep learning," *Lect. Notes Adv. Res. Electr. Electron. Eng. Technol.*, vol. 180, p. 185, Jan. 2019.
[28] Q. Li, Z. Yu, S. Qi, Z. He, S. Li, and H. Guan, "A recognition method of urine cast based on deep learning," in *Proc. Int. Conf. Syst., Signals Image Process. (IWSSIP)*, Jun. 2019, pp. 157–161.
[29] H. Xiang, Q. Chen, Y. Wu, D. Xu, S. Qi, J. Mei, Q. Li, and X. Liu, "Urine calcium oxalate crystallization recognition method based on deep learning," in *Proc. Int. Conf. Autom., Comput. Technol. Manag. (ICACTM)*, Apr. 2019, pp. 30–33.
[30] W. Liu, W. Li, and W. Gong, "Ensemble of fine-tuned convolutional neural networks for urine sediment microscopic image classification," *IET Comput. Vis.*, vol. 14, no. 1, pp. 18–25, Feb. 2020.
[31] T. Nagai, O. Onodera, and S. Okuda, "Deep learning classification of urinary sediment crystals with optimal parameter tuning," *Sci. Rep.*, vol. 12, no. 1, p. 21178, Dec. 2022.
[32] S. Dong, S. Zhang, L. Jiao, and Q. Wang, "Automatic urinary sediments visible component detection based on improved YOLO algorithm," in *Proc. Int. Conf. Comput. Vis., Image Deep Learn. (CVIDL)*, Jul. 2020, pp. 485–490.
[33] K. Li, M. Li, Y. Wu, X. Li, and X. Zhou, "An accurate urine erythrocytes detection model coupled faster RCNN with VggNet," in *Proc. Conf. Artif. Intell. Healthcare*, Oct. 2020, pp. 224–228.
[34] S. Yang, B. Fang, W. Tang, X. Wu, J. Qian, and W. Yang, "Faster R-CNN based microscopic cell detection," in *Proc. Int. Conf. Secur., Pattern Anal., Cybern. (SPAC)*, Dec. 2017, pp. 345–350.
[35] H. Uryu, O. Migita, M. Ozawa, C. Kamijo, S. Aoto, K. Okamura, F. Hasegawa, T. Okuyama, M. Kosuga, and K. Hata, "Automated urinary sediment detection for Fabry disease using deep-learning algorithms," *Mol. Genet. Metabolism Rep.*, vol. 33, Dec. 2022, Art. no. 100921.
[36] R. Kang, Y. Liang, C. Lian, and Y. Mao, "CNN-based automatic urinary particles recognition," 2018, *arXiv:1803.02699*.
[37] D. Goswami, H. Om Aggrawal, R. Gupta, and V. Agarwal, "Urine microscopic image dataset," 2021, *arXiv:2111.10374*.
[38] C. Tan, F. Sun, T. Kong, W. Zhang, C. Yang, and C. Liu, "A survey on deep transfer learning," in *Proc. Int. Conf. Artif. Neural Netw.* Cham, Switzerland: Springer, 2018, pp. 270–279.
[39] K. Simonyan and A. Zisserman, "Very deep convolutional networks for large-scale image recognition," 2014, *arXiv:1409.1556*.
[40] G. Huang, Z. Liu, L. Van Der Maaten, and K. Q. Weinberger, "Densely connected convolutional networks," in *Proc. IEEE Conf. Comput. Vis. Pattern Recognit. (CVPR)*, Jul. 2017, pp. 2261–2269.
[41] Y. Liang, R. Kang, C. Lian, and Y. Mao, "An end-to-end system for automatic urinary particle recognition with convolutional neural network," *J. Med. Syst.*, vol. 42, no. 9, pp. 1–14, Sep. 2018.
[42] M. Kaneko, K. Tsuji, K. Masuda, K. Ueno, K. Henmi, S. Nakagawa, R. Fujita, K. Suzuki, Y. Inoue, S. Teramukai, E. Konishi, T. Takamatsu, and O. Ukimura, "Urine cell image recognition using a deep-learning model for an automated slide evaluation system," *BJU Int.*, vol. 130, no. 2, pp. 235–243, Aug. 2022.
[43] C. Han, K. Murao, T. Noguchi, Y. Kawata, F. Uchiyama, L. Rundo, H. Nakayama, and S. Satoh, "Learning more with less: Conditional PGGAN-based data augmentation for brain metastases detection using highly-rough annotation on MR images," in *Proc. 28th ACM Int. Conf. Inf. Knowl. Manag.*, Nov. 2019, pp. 119–127.
[44] M. Erten, P. D. Barua, I. Tuncer, S. Dogan, M. Baygin, T. Tuncer, R.-S. Tan, and U. R. Acharya, "Swin-LBP: A competitive feature engineering model for urine sediment classification," *Neural Comput. Appl.*, vol. 35, no. 29, pp. 21621–21632, Oct. 2023.
[45] T. Li, D. Jin, C. Du, X. Cao, H. Chen, J. Yan, N. Chen, Z. Chen, Z. Feng, and S. Liu, "The image-based analysis and classification of urine sediments using a LeNet-5 neural network," *Comput. Methods Biomechanics Biomed. Eng., Imag. Visualizat.*, vol. 8, no. 1, pp. 109–114, Jan. 2020.

SANIA AKHTAR received the B.S. (Hons.) and M.S. degrees in software engineering from the COMSATS University of Information and Technology, Islamabad, Pakistan, in 2017 and 2020, respectively. She is currently pursuing the joint Ph.D. degree in computer sciences with the Ghulam Ishaq Khan Institute of Engineering Sciences and Technology (GIK), Pakistan, collaborating with Kutahya Dumlupinar University, Turkey, on urine sediment analysis for kidney and renal infections. Before joining the Ph.D. degree, she was a Research Assistant with the Shaheed Zulfikar Ali Bhutto Institute of Science and Technology (SZABIST) on healthcare and artificial intelligence projects. She was involved in an HEC project under the National Center of Artificial Intelligence. Her research interests include healthcare, medical image processing, computer vision, and deep learning. She has received several awards, including an Award of Honors during her B.Sc. Program, a Full University Scholarship for the Ph.D. degree, and two Deans' Roll of Honor Awards, in 2022, for outstanding academic performance with GIK.

MUHAMMAD HANIF received the M.Sc. degree in signal processing from Tampere University of Technology, Tampere, Finland, and the Ph.D. degree in computer vision from the College of Engineering and Computer Science, The Australian National University, Canberra, ACT, Australia. He was associated with the Computer Vision and Robotics Research Group, National ICT Australia (NICTA), DTAT61. He was also associated with Istituto di Scienza e Tecnologie dell'Informazione "A. Faedo," CNR. Currently, he is an Assistant Professor with the Faculty of Computer Science and Engineering, Ghulam Ishaq Khan Institute of Engineering Sciences and Technology, Pakistan. He is also associated with the Kobayashi Research Laboratory, Information Technology Center, The University of Tokyo. His main research interests include blind image deconvolution and sparse image processing. He was a recipient of European Research Consortium for Informatics and Mathematics (ERCIM) Fellowship for his postdoctoral research work with Italian National Research Council (CNR), Pisa, Italy.

AHMAR RASHID enjoys about 20 years of industrial and research and development experience. His professional experiences include preparing functional specifications, designing and implementing software for financial applications, diagnosis, troubleshooting, and resolution of customer's technical issues. His core research interests include the performance analysis of optimization algorithms for static and dynamic image reconstruction using electrical impedance tomography (EIT) with application in industrial process monitoring and medical imaging. His Ph.D. thesis was on the application of oppositional biogeography-based optimization, which is one of the most recently developed evolutionary algorithms, to solve boundary estimation problems using EIT. The specific problem solved was estimating the size and location of the human heart while a patient is told to hold his/her breadth.

KHURSHEED AURANGZEB (Senior Member, IEEE) received the B.S. degree in computer engineering from the COMSATS Institute of Information Technology, Abbottabad, Pakistan, in 2006, the M.S. degree in electrical engineering (system on chip design) from Linkoping University, Sweden, in 2009, and the Ph.D. degree in electronics design from Mid Sweden University, Sweden, in June 2013. He is currently an Associate Professor with the Department of Computer Engineering, College of Computer and Information Sciences, King Saud University (KSU), Riyadh, Saudi Arabia. He has authored or coauthored more than 90 publications, including IEEE/ACM/Springer/Hindawi/MDPI journals and flagship conference papers. He has obtained more than 15 years of excellent experience as an Instructor and a Researcher in data analytics, machine/deep learning, signal processing, electronics circuits/systems, and embedded systems. He has been involved in many research projects as a principal investigator and a co-principal investigator. His research interests include embedded systems, computer architecture, signal processing, wireless sensor networks, communication, and camera-based sensor networks, emphasizing big data and machine/deep learning with applications in smart grids, precision agriculture, and healthcare.

EJAZ AHMAD KHAN is currently a Medical Doctor, a Public Health Academician, a Researcher, and a Consultant with a post-graduation in primary health care/public health and fellowship in public health. He has more than 23 years' experience of in teaching training, research, consultancies, and program management in public health, epidemiology, communicable, non-communicable diseases and injuries, nutrition, and environmental health. He has published extensively with more than 200 published researched items in international journals with a H-index of 78 and i10 of 113. In 2022, he ranked among the world's 100 scientists with the top rank in his professional disciplines within Asia.

HAMDI MELIH SARAOGLU was born in Isparta, Turkey, in 1971. He received the B.C. degree in electronics engineering from Erciyes University, Kayseri, Turkey, in 1993, the M.S. degree in electrical and electronics engineering from Kütahya Dumlupınar University, Kütahya, Turkey, in 1995, and the Ph.D. degree in electrical and electronics engineering from Sakarya University, Sakarya, Turkey, in 1998. He was a Research Assistant, from 1993 to 2002, an Assistant Professor, between 2002 to 2011, an Associate Professor, until 2018, and has been a Professor with the Department of Electrical and Electronics Engineering, Kütahya Dumlupınar University, since 2018. He founded the Neurotechnology Education Application and Research Center, in 2022. He founded a medical startup company, in 2023. In this company, he designed devices, such as a medical infusion pump, urine chemical strip reader, urine sediment analyzer, and dosage pump. His research interests include biomedical signal processing and image processing.

KAMRAN JAVED received the B.Sc. degree (Hons.) in electronic engineering and the M.Sc. degree in computer engineering from the University of Engineering and Technology (UET) Taxila, Taxila, Pakistan, in 2012 and 2014, respectively, and the Ph.D. degree in electronic and computer engineering from Sungkyunkwan University, South Korea, in 2020. He was a Lecturer with the Electronic Engineering Department, UET Taxila, from 2013 to 2016, and an Assistant Professor with the Ghulam Ishaq Khan Institute of Engineering Sciences and Technology, Topi, Pakistan, from 2020 to 2021. He is currently an AI Research Scientist with the National Center of Artificial Intelligence (NCAI), Creativity Research Department, Riyadh, Saudi Arabia. His research interests include generative adversarial networks and their application to computer vision for image unmosaicing and object removal. His awards and honors include the Award of Honors for a B.Sc. degree, in 2012, the University Scholarship for an M.Sc. degree, in 2012, and the Higher Education Commission Scholarship for the Ph.D. degree (abroad) from HEC, Pakistan, in 2016.